The 6th International Supercritical CO_2 Power Cycles Symposium
March 27 - 29, 2018, Pittsburgh, Pennsylvania

Dynamic modeling and transient analysis of a molten salt heated recompression supercritical CO_2 Brayton cycle

Jinyi Zhang
Research engineer
EDF R&D China
Beijing, China

Zijiang Yang
Research engineer
EDF R&D China
Beijing, China

Yann Le Moullec
Chief engineer
EDF R&D China
Beijing, China

ABSTRACT

Supercritical CO_2 (S-CO_2) Brayton cycle is a high-potential power generation technology with high thermal efficiency and compact machineries, nevertheless questions arise regarding its operability and flexibility. Dynamic modeling and simulation is an important tool to understand the cycle performance under transient operation and to help design dedicated control strategies.

In this work, a dynamic physical model of a 100MWe S-CO_2 Brayton recompression cycle is built in Modelica language implemented in Dymola®. The developed model is designed for the application of concentrated solar power plant with thermal storage; therefore, a molten salt heat exchanger and an air cooler are selected, respectively, as the heat and cold source. Turbo-machineries are modeled through performance map generated from mean-line turbine and compressor models.

A part-load scenario from 100% to 50% is studied in this work. Based on this model, molten salt temperature control, main compressor inlet temperature and pressure control are implemented to insure the operation safety and stability of equipment and cycle. Finally, 2 different part-load control options are simulated and analyzed, and based on their characteristics, a new control strategy is proposed by combining the advantages of these two control options, which improves the control response speed and net cycle efficiency at low load level.

INTRODUCTION

CO_2 exhibits many attracting characteristics for power generation industry. It is abundant and inexpensive, less corrosive compared to water at the same high temperature [Ahn 2015] with easily-achievable critical point (30.98℃, 7.38Mpa). It also shows a very good thermal stability up to 1500℃. Brayton cycle operating with supercritical CO_2 (S-CO_2) benefits from the real gas behavior of CO_2 in the vicinity of the Andrews curve, which leads to the reduction of specific volume and therefore of compression work in the cycle. More reduction of compression work can also be achieved when CO_2 is compressed closer to its critical point, as the fluid becomes more incompressible [Ahn 2015]. This mechanical effect, i.e. the significant reduction of compression work, results in higher thermal efficiency of S-CO_2 Brayton cycle compared to other working fluid for Brayton cycle, e.g. helium or air. As the S-CO_2 Brayton cycle operates above the critical point, with a minimum pressure of ~7.4MPa (Steam Rankine cycle minimum pressure is only a few kPa), the fluid remains dense throughout the entire system. Therefore, the volume of turbo-machineries is reduced significantly. Besides, the system layout is also simpler, e.g. a 300MWe power plant only requires one turbine with 4 stages [Dostal 2004]. S-CO_2 Brayton cycle with higher thermal efficiency, high power density and compact turbo-machinery, could potentially reduce the capital expenditure (CAPEX) and then the levelized cost of electricity (LCOE) for power plant.

As a low maturity technology, the operation and control of S-CO_2 Brayton cycle need to be carefully studied before its full application in power generation. Part-load scenarios occur frequently during the operation of modern power plant, therefore a better understanding of part-load operation and assessment of different control strategies is critical for the optimization of global operation and cycle performance at part load.

Dynamic modeling and simulation is a useful and efficient tool during the development of control strategies. In this work, a dynamic physical model of a 100MWe S-CO_2 Brayton recompression cycle design is built in Dymola®. The developed model is designed for the application of concentrated solar

power plant with molten salt for the thermal storage, therefore a molten salt heat exchanger and an air condenser are selected, respectively, as heat and cold source. Molten salt outlet temperature control, main compressor inlet temperature and pressure control are implemented as basic controllers to insure the operation safety and stability of equipment and cycle. This paper focuses on testing different part-load control strategies by comparing two control options. The key cycle parameters during control process are shown and analyzed, which helps to understand the control characteristics of these two options and their impact on cycle transient behaviors and performance. Based on the characteristics of these two control options shown by the simulation results, a new control strategy is proposed by combining the advantages of these two control options.

SYSTEM DESIGN

Many different CO_2 Brayton cycle layouts have been proposed and analyzed [Dostal 2004, Ahn 2015]. Among these layouts, the recompression cycle illustrated in Figure 1 is considered to a good layout for an indirect-heated cycle with a balance between thermal efficiency and system complexity [Dostal 2004]. Therefore, the recompression layout is selected for the system.

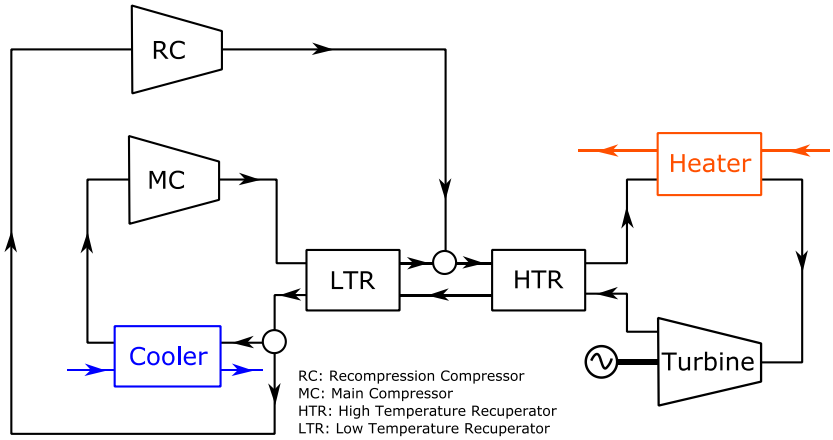

Figure 1 Supercritical CO2 Brayton cycle recompression layout

The cycle is designed for a net electric power output of 100MWe. Due to the fact that the highest temperature acceptable for molten salt is 560℃, then with a 20℃ temperature pinch for heat exchanger design, this turbine inlet temperature is selected to be 540℃. As a preliminary study, the minimum cycle temperature and pressure are selected to be 35℃ and 8MPa respectively, which is not so close to the critical point, in order to avoid too much instability of cycle operation. More details about cycle design parameters are given in Table 1.

Table 1 Key 100MWe CO2 Brayton cycle design parameters

Item	Unit	Value
Turbine inlet pressure	bar	201
Main compressor inlet pressure	bar	80
Turbine inlet temperature	℃	540
Main compressor inlet temperature	℃	308.15
Turbine mass flow rate	kg/s	1326
Recompression split ratio	%	36.62
Turbine power	MWe	153.1
Main compressor power	MWe	17.8
Recompression compressor power	MWe	29.9
Net power output	MWe	100

Molten salt/CO_2 shell-tube heat exchanger is used for the heater, air cooler is used for cooling the CO_2 flow,

Printed Circuit Heat Exchanger (PCHE) with semi-circular straight channels is used for the recuperation of turbine outlet heat. The preliminary design of these three heat exchangers is given by the in-house tools. Axial compressor is used for main compressor and recompression compressor, and the design is given by a mean-line compressor design model based on Aungier's work [Aungier 2003]. The turbine is also axial and its design is given by a mean-line turbine design model mainly based on the work of Jean-Michel Tournier [Tournier 2010].

SYSTEM MODEL

The model is built in Dymola® from Dassault Systemes (Dassault Systemes, France), a commercial multi-physics modeling and simulation platform based on programming language Modelica. The fluid thermodynamic properties are calculated by NIST REFPROP®.

1. Mass, Energy and Momentum Balance

The mass, energy and momentum equations are the fundamental laws that govern the thermal-hydraulic behaviors of fluid. For thermal process modeling, zero-dimension modeling approach is used. Therefore, no specialization of phenomenon is considered in the component model for mass, energy and momentum balance. These three equations are simplified for zero-dimension modeling and listed in Eq. (1), Eq. (2), Eq. (3):

$$V \cdot \left(\frac{\partial \rho}{\partial p}\frac{\partial p}{\partial t} + \frac{\partial \rho}{\partial h}\frac{\partial h}{\partial t}\right) = \sum Q_{in,i} - \sum Q_{out,i} \tag{1}$$

$$V\left(\left(h\frac{\partial \rho}{\partial p} - 1\right)\frac{\partial p}{\partial t} + \left(h\frac{\partial \rho}{\partial h} + \rho\right)\frac{\partial h}{\partial t}\right) = \sum Q_{in,i} \cdot h_{in,i} - \sum Q_{out,i} \cdot h_{out,i} \tag{2}$$

$$L\frac{dQ}{dt} = A \cdot \left(p_{in} - p_{out} - \Delta p\right) \tag{3}$$

Q represents mass flow rate, h represents specific enthphy and p represents pressure. Subscript in and out mean component inlet and outlet properties, all the properties without subscript means the medium volume average property in the component.

2. Pressure Drop Model

The pressure drop is considered in the current work only in the heat exchanger in the form of friction pressure loss. The friction pressure loss is due to the molecular and turbulent viscosity of fluid. It is closely related to fluid passage geometry such as length L and hydraulic diameter D, passage surface roughness ε and flow characteristics such as flow velocity v and density ρ. To calculate the friction pressure loss Δp_{fr} through a regular channel (or pipe/duct), the Darcy-Weisbach equation [Brown 2002] (Eq. (4)) is considered the best empirical relation for friction pressure loss.

$$\Delta p = f_D \frac{L}{D}\frac{\langle v \rangle^2}{2\rho} \tag{4}$$

Where f_D is the Darcy friction factor. $\langle v \rangle$ is the average flow velocity in the cross section of flow passage. The Darcy friction factor is critical to evaluate the friction pressure loss, so it has to be determined in an appropriate way. Depending on flow behavior and the relationship between Reynolds number and flow resistance, Nikuradse identifies four different flow zones by experiment [Nikuradse 1933]: laminar zone, critical zone, transition zone and full turbulent zone. These four zones have been extensively used as a reference for the development of correlations since then, which are also adopted in this model.

Within the Laminar zone, i.e. $\mathrm{Re} < 2000$, the roughness has no impact on Darcy friction factor. In this region, all the curves with different roughness coincide with the curve of smooth pipe. A widely-accepted and recommended correlation [Nikuradse 1933, Idel'chik 1966, Hesselgreaves 2001] for laminar zone is used:

$$f_D = \frac{64}{\mathrm{Re}} \tag{5}$$

Eq. (5) is recommended for circular pipes, another correlation in Eq. (6) is proposed by Hesselgreaves [Hesselgreaves 2001] for semi-circular channel which is used for semi-circular Printed Circuit Heat Exchanger (PCHE):

$$f_D = \frac{63.12}{\mathrm{Re}} \tag{6}$$

Within the critical zone, i.e.$2000 < \mathrm{Re} < 4000$, f_D rises with respect to Reynolds number. At the beginning of this zone, a quasi-linear relationship independent of roughness is observed in Nikuradse's experimental result until 80% of this zone, then the slope of curve decreases until the end of critical zone and the effect of roughness starts to appear to match the beginning of transition zone. No practical correlation has been found in the literature. For simplification and without introducing significant error, a linear interpolation between the laminar zone correlation and transition zone correlation is done. This interpolation also avoids a lot of mathematical work to create one correlation which gives a precise match to the beginning point of transition zone which is highly roughness dependent.

Within the transition zone, f_D first decreases following the smooth pipe curve then detaches from it and continues to decrease until a local minimum and then increases. The experimental results from Nikuradse [1933] and Shockling [2006] confirms this variation trend. Afzal [2007] proposed an inflectional roughness prediction correlation (Eq. (7)) with $j = 11$ which predicts the transition trend and corresponds well to the experiments result on commercial pipes. Therefore, Afzal equation will be used in the modeling in these two zones.

$$\frac{1}{\sqrt{f_D}} = -2\log_{10}\left(\frac{2.51}{\mathrm{Re}\sqrt{f_D}} + \frac{\varepsilon}{3.7D_h}\exp\left(-j\frac{5.66}{\mathrm{Re}\sqrt{f_D}}\frac{r}{\varepsilon}\right)\right) \tag{7}$$

Within the fully turbulent zone, Darcy friction factor is independent of Reynolds number, depending only on the roughness. The Darcy friction factor given by Afzal equation within this zone reaches a stable value which depends on the roughness. This equation provides also reasonable accuracy compared to the experiment results [Sletfjerding 1999].

3. Heat Transfer Model

Heat transfer in the heat exchanger is realized mainly by conduction and convection. Radiation is not taken into account. Heat conduction is used mainly for the wall heat transfer modeling, which is modeled as in Eq. (8).

$$q = \frac{(T_2 - T_1)}{\delta / k} \tag{8}$$

Where k is thermal conductivity of the wall material, δ is the wall thickness.

Convective heat transfer is the heat transfer by the movement of fluids. The basic relationship for convective heat transfer is described as in Eq. (9)

$$q = h_{tc} \cdot S \cdot (T_{fluid} - T_{wall}) \tag{9}$$

Where q is the heat transferred from fluid to wall per unit time, S is the total heat transfer surface, h_{tc} is the heat transfer coefficient. The commonly way to find HTC is by determination of Nusselt number Nu, then based on the relationship in Eq. (10) to find h_{tc}.

$$Nu = \frac{h_{tc}D}{k} \tag{10}$$

Where k is the thermal conductivity of fluid.

The Nusselt number is calculated depending on the flow conditions. For laminar flow, i.*e.* $Re < 2000$, Hesselgreaves [Hesselgreaves 2001] proposed to use 4.3636 for circular duct and 4.089 for semi-circular duct (the channels in PCHE is semi-circular). For turbulent flow, i.e.$\mathrm{Re} > 4000$, Dostal [Dostal 2004] and

Carstens [Carstens 2006] proposed to use the Gnielinski Correlation in Eq. (11) which is valid for $0.5 \leq Pr \leq 2000$ and $3000 \leq Re \leq 5 \times 10^6$. This working condition covers most of our operation condition.

$$Nu = \frac{\left(f_D/8\right)\left(\mathrm{Re}-1000\right)\mathrm{Pr}}{1+12.7\left(f_D/8\right)^{1/2}\left(\mathrm{Pr}^{2/3}-1\right)}\left(1+\left(\frac{D_h}{L}\right)^{2/3}\right) \tag{11}$$

Where the Darcy friction factor f_D is calculated by Colebrook-White equation. Because the Colebrook-White equation is implicit, which may make the system stiffer and difficult to solve, therefore an approximation proposed by Chen [Chen 1979] is applied to calculate f_D. Chen approximation is shown below in Eq. (12)

$$\frac{1}{\sqrt{f_{fa}}} = 3.48 - 1.7372\ln\left(2\frac{\varepsilon}{D} - \frac{16.2426}{\mathrm{Re}}\ln\left(\frac{\left(2\varepsilon/D\right)^{1.1098}}{6.0983} + \left(\frac{7.149}{\mathrm{Re}}\right)^{0.8981}\right)\right) \tag{12}$$

The result should be multiplied by 4 to get the Darcy friction factor.

All the correlations above were proposed for normal turbulent operation condition, not for supercritical conditions nor for CO_2. Based on the Supercritical CO_2 experimental dataset (Pressure ranges from 7.4 to 8.8Mpa, Temperature ranges from 20 to 40℃), Gupta [Gupta 2012] proposed one wall temperature-dependent correlation which shows a good accuracy. Since the air condenser works close to the condition where the dataset are collected, the convective heat transfer in air condenser will use Gupta correlation for turbulent zone at the CO_2 side. Gupta correlation is shown in Eq. (13)

$$Nu = 0.0038\,\mathrm{Re}_w^{0.96}\,\mathrm{Pr}_w^{-0.14}\left(\frac{\rho_w}{\rho_b}\right)^{0.84}\left(\frac{k_w}{k_b}\right)^{-0.75}\left(\frac{\mu_w}{\mu_b}\right)^{-0.22} \tag{13}$$

Where subscript w and b means wall temperature and fluid bulk dependent fluid properties. Here, Re_w is calculated based on wall temperature dependent property and same for Pr_w. For the other equipment, the conventional Gnielinski correlation is used.

Between the laminar zone and turbulent zone, the transition zone (which is different from the one defined in friction pressure loss section) is correlated by linear interpolation between laminar and turbulent zone.

For tube flow, following the recommendation of Ray [Ray 2010], the overall heat transfer coefficient is calculated as in Eq. (14)

$$\frac{1}{U} = \frac{1}{h_{tc,o}} + \frac{1}{h_{od}} + \frac{D_o\ln\left(D_o/D_i\right)}{2k} + \frac{D_o}{D_i}\frac{1}{h_{id}} + \frac{D_o}{D_i}\frac{1}{h_{tc,i}} \tag{14}$$

Where $h_{tc,i}$ and $h_{tc,o}$ are the heat transfer coefficients for two sides, h_{id} and h_{od} is inside and outside dirt coefficients, D_i and D_o are inside and outside diameters.

4. Heat exchanger

Three types of heat exchangers are modeled, including semi-circular CO_2/CO_2 printed circuit heat exchanger (PCHE), molten salt/CO_2 shell-tube heat exchanger and air/CO_2 cooler. The same modeling methodology is used for these three heat exchangers. The model is composed of two channel models connected through thermal exchanger port to realize the heat exchange (as illustrated in Figure 2). One channel model is for the high-temperature flow and another one for low-temperature flow. Every channel model is discretized into N sections (N is defined by the user). The discretized equivalent model representation is illustrated in Figure 2. N should be carefully selected to have a reasonable balance between accuracy and simulation time.

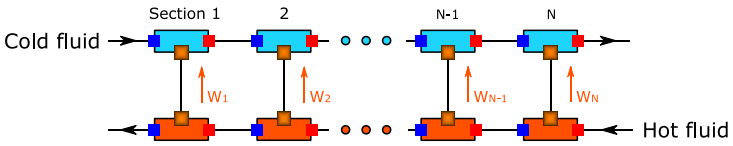

Figure 2 PCHE discretized equivalent model representation

The mass, momentum and energy balance equations in every section follows exactly the same form as those defined in Eq. (1), Eq. (2), Eq. (3).

The heat transfer model applied is given by the heat transfer model defined in Section [3.Heat transfer model]. The pressure drop applied is given by the pressure drop model defined in Section [2.Pressure Drop Model]. When calculating friction pressure drop, channel roughness is required. For PCHE channel, the roughness used comes from the roughness of chemical etched stainless steel in Satish's work [2003] which is 1.9 μm. For other channels, the normal commercial pipe roughness is used.

5. Turbo-machinery

Turbo-machinery has an important impact on the global cycle behavior, therefore a detailed design and off-design approach is adopted to reflect as close as possible the real performance of turbo-machinery, which takes into account the mass flow rate, rotation speed, inlet temperature and pressure. The final compressor and turbine modeling in Dymola® follows the procedure as shown in Figure 3:

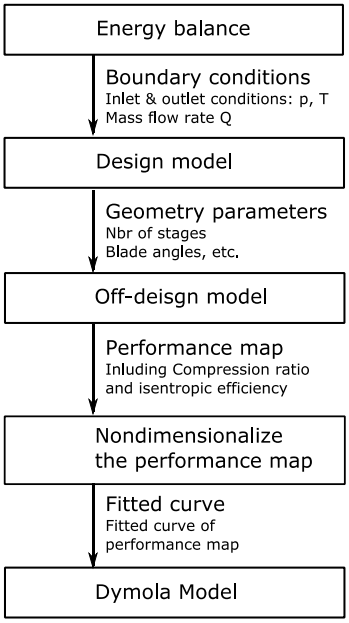

Figure 3 Turbo-machinery modeling methodology

1. Energy balance diagram is obtained from steady-state simulation, which gives the necessary boundary conditions at design point for the design model;
2. Based on the boundary conditions given by energy balance, the turbo-machinery design model gives a basic design, i.e. geometry parameters of turbo-machinery. The axial compressor design is given by a mean-line compressor design model based on Aungier's work [Aungier 2003]. The axial turbine design is given by a mean-line turbine design model mainly based on the work of Jean-Michel Tournier [Tournier 2010].
3. The off-design model generates the performance map which includes the isentropic efficiency η and compression/expansion ratio τ or another equivalent isentropic enthalpy change Δh_i. The off-design models are based on the same model as design model, except that for the off-design model, the geometry parameters are fixed during the calculation.

4. The turbo-machinery off-design behavior depends on working fluid, mass flow rate, rotation speed, inlet pressure and temperature. Since it is difficult for Dymola® to deal with high-dimension table, The Nondimensionalization method of the performance map proposed by Dyreby [Dyreby 2014] is used. The flow coefficient ϕ is corrected by rotation speed, modified enthalpy change ψ^* and modified isentropic efficiency η^* are used to represent the turbo-machinery performance. a_1, a_2, a_3, a_4 are empirical coefficients depending on the design of turbo-machinery.

$$\phi^* = \frac{\dot{m}}{\rho U D^2}\left(\frac{N}{N_{design}}\right)^{a_1} \tag{15}$$

$$\psi^* = \frac{\Delta h_i}{U^2}\left(\frac{N}{N_{design}}\right)^{\left(a_2\cdot\phi^*\right)^{a_3}} \tag{16}$$

$$\eta^* = \eta\left(\frac{N}{N_{design}}\right)^{\left(a_2\cdot\phi^*\right)^{a_4}} \tag{17}$$

6. Basic Control Loop

Besides the part-load controller to be implemented later, two basic Proportional-Integral-Derivative (PID) controllers are included in the cycle to insure safe and stable operation of equipment and cycle, as illustrated in Figure 4. These two controllers work in parallel with the part-load controller to be implemented.

- Molten salt outlet temperature (MSOT) control: this controller is used to control the temperature of the molten salt which flows into the cold tank, by regulating the molten salt mass flow rate through the heat exchanger. When the temperature of molten salt that flows into the cold tank is higher than the reference temperature, the mass flow rate decreases.
- Main compressor inlet temperature (MCIT) control: this is realized by controlling the air cooler fan rotation speed. When MCIT is higher than the reference temperature, the air cooler fan rotation speed increases, the air flow velocity increases, then the heat in the CO_2 flow can be better evacuated.

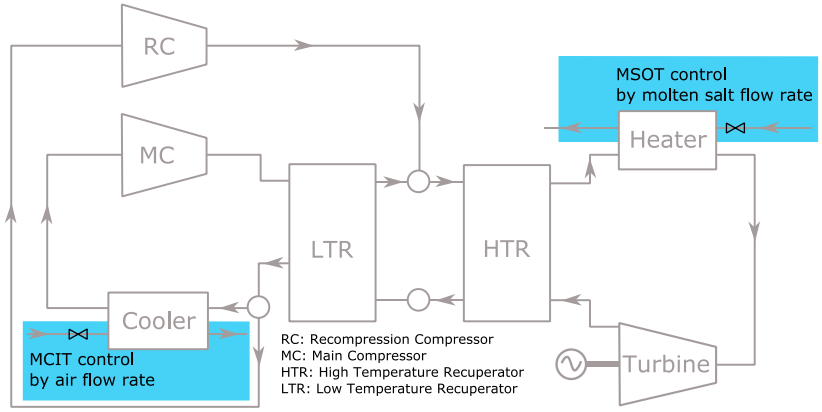

Figure 4 Three basic control loops

The MCIT control are used to keep CO_2 above the critical point and protect the main compressor from operating in the two-phase region. Moreover, the main compressor performance is very sensitive to the inlet condition, a more stable inlet condition will increase the stability of the cycle.

PART-LOAD CONTROL RESULT

1. Inventory Control

Part-load control by Inventory is realized by two CO_2 tanks: one with lower pressure (7.5MPa) is connected

to the downstream side of main compressor and the other with higher pressure (10MPa) to the upstream of main compressor. These two tanks are assumed to maintain constant pressure during inventory charging and discharging. When the load is required to decrease, the cycle inventory should be discharged from the cycle, i.e. the valve between the low-pressure tank and cycle should be opened. As a result of inventory discharge, turbine inlet pressure and mass flow rate decreases, which leads to the load reduction. The main compressor inlet pressure (MCIP) protection mechanism is also implemented into the control logic of inventory control, which works as a constraint for inventory control, in order to prevent the CO_2 pressure from falling below the critical pressure. A safe working zone is set by the protection mechanism, when the MCIP is in the safe zone, no intervention is applied to the standard inventory control. When the MCIP is lower than the safe zone, the discharge rate is reduced and when reaching 7.4MPa, the discharge rate is set to zero because this is very close to the critical pressure. When MCIP is higher than the safe zone, the injection rate will be reduced.

Since the current work is dedicated to study the impact of different control options on cycle performance, a simplified inventory control system design of two tanks with constant pressure is adopted. This is also to avoid the complex modeling and control system design for the mass management system, but an optimized inventory control system will be considered in the future work.

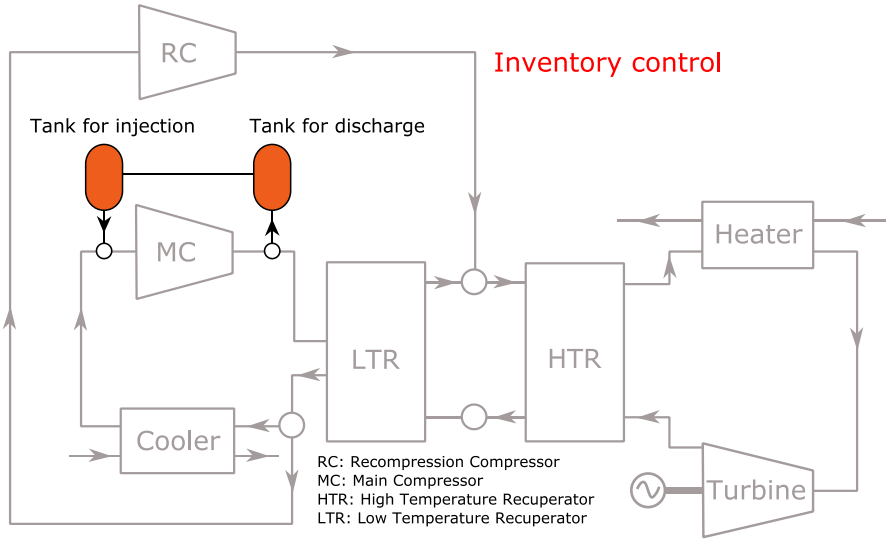

Figure 5 Inventory Control

As shown in Figure 6, a step reference load level signal is sent to the controller, which changes from 100% load to 50% load at 200s, the inventory control takes action immediately, the load level starts to decrease then approaches the reference load level. The black points in Figure 7 gives the relation between load level and net cycle efficiency during the transient process, which shows that the net cycle efficiency decreases monotonically with load level. At 100% load, the cycle gives a net efficiency of 42.41%, at 50% load, the net efficiency decreases to 37.40%. This efficiency reduction of 5.01% points is higher than that of ultra-supercritical Rankine cycle which is around 2.5% (data from one of the thermal power plants owned by EDF). The efficiency reduction mainly comes from a reduced turbine inlet temperature (TIT) and pressure (TIP) as shown in Figure 8 and Figure 9. Another cause is that the PCHE temperature pinch increases, e.g. the pinch at the high temperature end of LTR increases from 12.35℃ to 14.77℃ at 50% load as shown by Figure 11, which has a negative impact on the PCHE heat exchange effectiveness.

TIT increases by 2.5 degrees when the control action starts, as a result of CO_2 flow rate reduction in the molten salt heat exchanger. In order to protect the turbine from TIT going above 540℃, it is necessary to add a TIT protection control by bypassing the flow from main compressor outlet to the turbine inlet. When the load level continues to decrease, TIT reaches a minimum of 524℃ which is 16℃ lower than the design value. This mainly comes from the ineffective heat exchange in the molten salt heat exchanger, since the flow velocity of both molten salt and CO_2 decreases significantly, which leads to the reduction of overall heat transfer coefficient.

In order to improve the efficiency by maintain the TIT temperature near the design value, the MSOT control could be replaced by TIT control, and the TIT is controlled by manipulating molten salt flow rate, the red points in Figure 7 shows that the net efficiency at 50% load is increased from 37.40% to 38.11%. The efficiency during transition is similar with the MSOT control solution until 60% load level. But the molten salt outlet temperature is increased to 440℃ at 50% load, 25℃ higher than the designed cold tank molten salt storage temperature, which imposes challenges for the molten salt storage management.

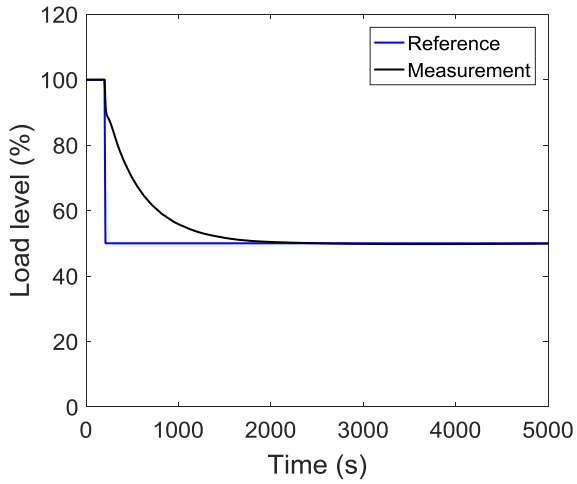

Figure 6 Reference load signal and measured power output

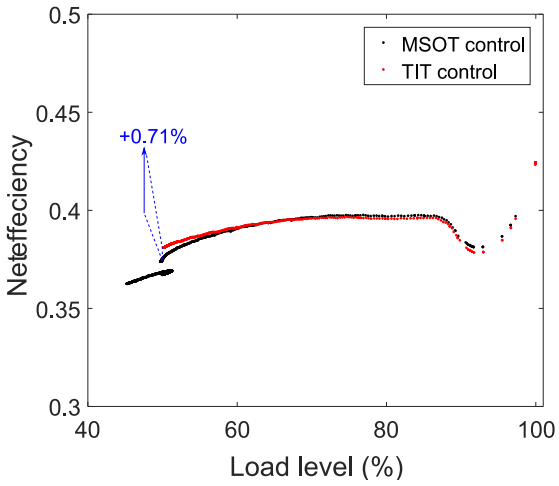

Figure 7 Load level and net efficiency

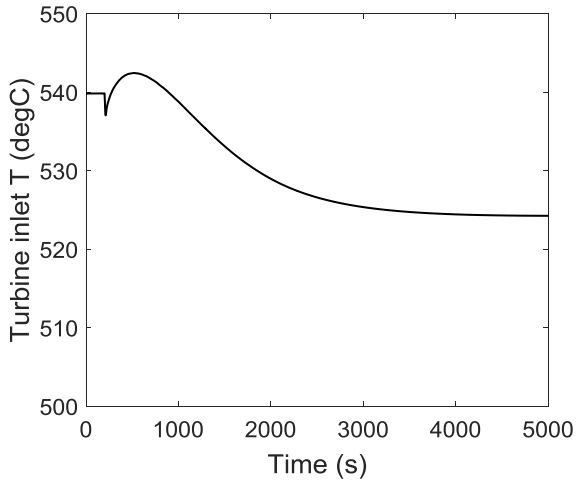

Figure 8 Turbine inlet temperature variation

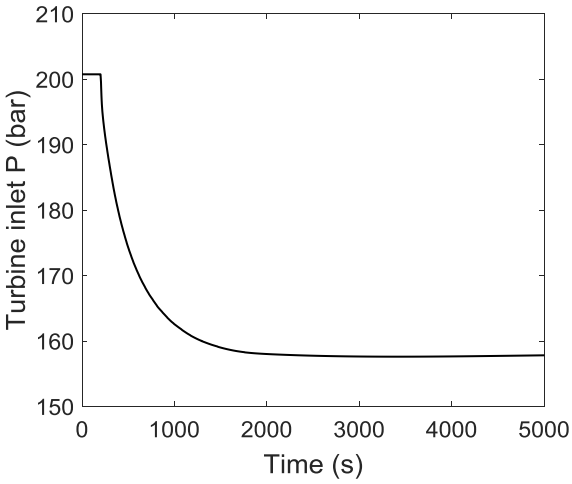

Figure 9 Turbine inlet pressure variation

Due to the effective MCIP protection mechanism, as shown in Figure 10, the MCIP stays in the safe region, but still very close to the critical pressure. Attention should be paid to inventory control when reaching lower load level. This protection mechanism limits also the control reaction speed, which puts a constraint on the discharge rate.

50% load reduction leads to a net cycle inventory discharge of 37.2 tons, 24% of initial inventory in the cycle. The huge amount discharged from the cycle also limits the inventory control application to lower level of load.

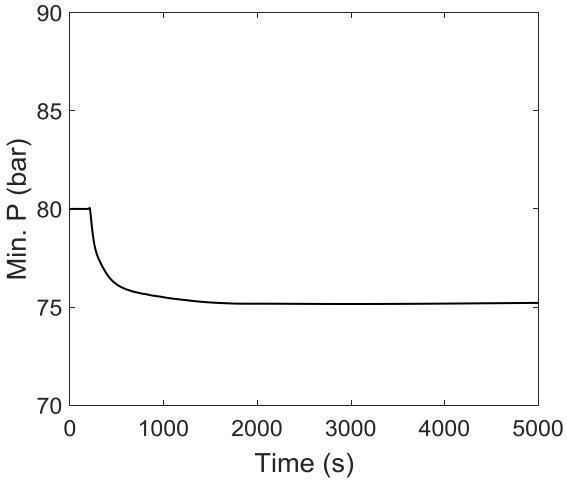

Figure 10 Cycle minimum pressure

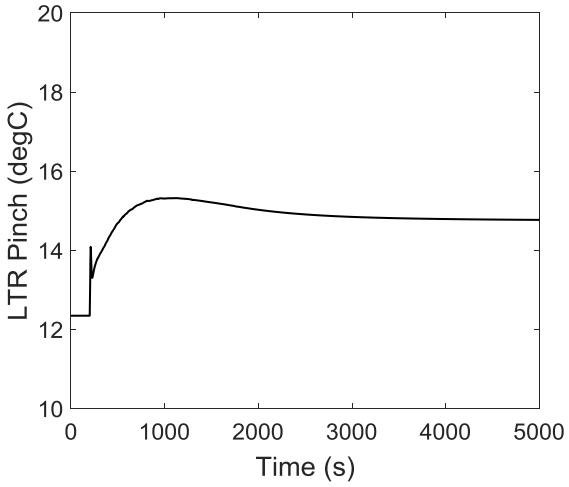

Figure 11 LTR high end temperature pinch

2. HTR & Heater & Turbine Bypass Control

This control is realized by bypassing the HTR, molten salt heat exchanger and turbine, as illustrated in Figure 12.

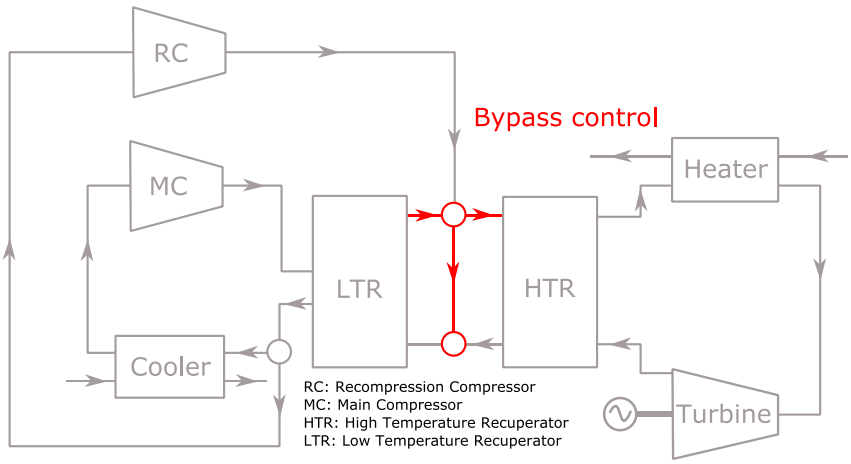

Figure 12 HTR & Heater & Turbine Bypass Control

With a step load reference signal, this bypass control reacts very fast, much faster than inventory control, as shown in Figure 13. Due to the fast reaction of this controller, only a few data points are captured for high load level, which shows an interesting efficiency transient behavior. But this region is too short in time, so the efficiency does not have an important impact on off-design behavior. When reaching 55% load level, the efficiency decreases monotonically with load level. Compared to inventory control, the net efficiency at 50% load is much lower, only 27.51%, and it shows also a faster decreasing rate when the load level decreases. The efficiency reduction comes from the fact that the compressor energy consumptions do not change significantly for 100% and 50% load level but in the meanwhile the turbine output are cut significantly to match the 50% load level.

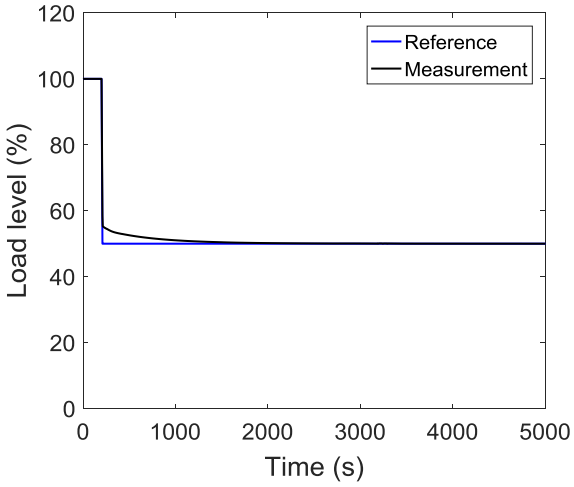

Figure 13 Reference load signal and measured power output

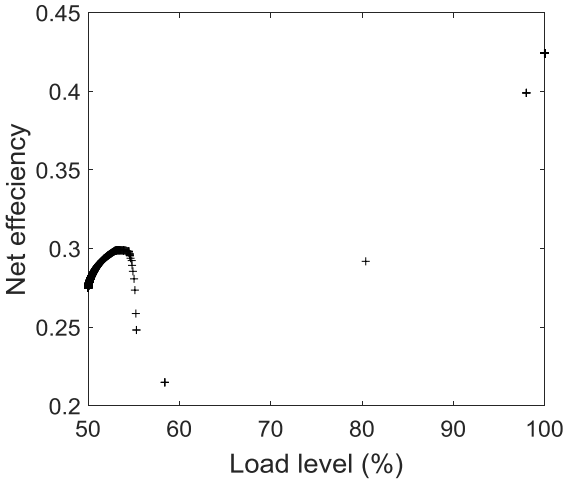

Figure 14 Load level and net efficiency

Due to the effective bypass, the turbine mass flow rate decreases from 1325kg/s to 1058kg/s in 150s, but the molten salt temperature control cannot react fast enough to the drastic mass flow rate change, as a result, the molten salt outlet temperature have an overshoot of 428℃, 13℃ higher than the set value. TIT also have small overshoot of 6℃, which remains in the safe region of turbine operation.

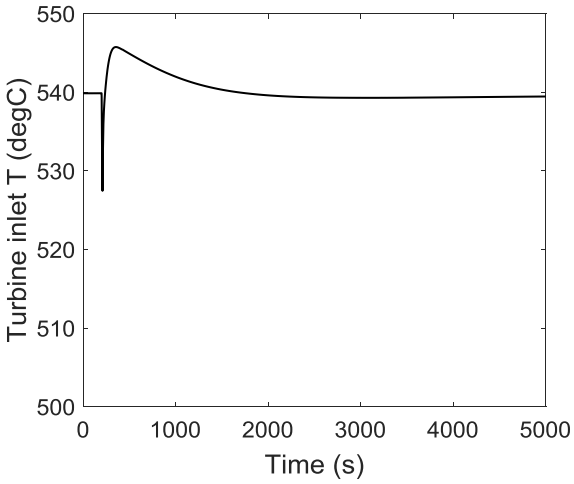

Figure 15 Turbine inlet temperature

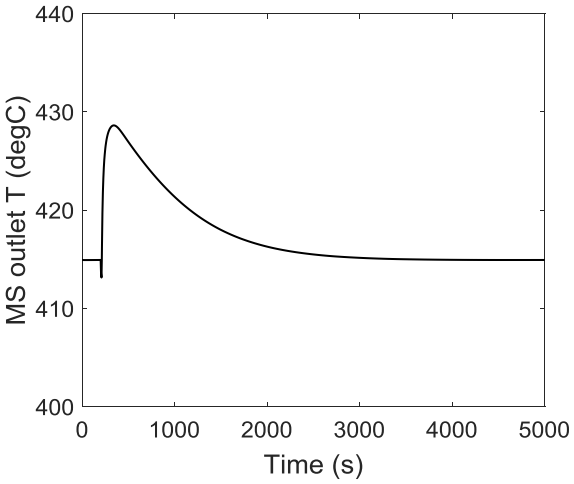

Figure 16 Temperature of the molten salt that flows into the cold tank

This bypass control does not put a big challenge on the minimum pressure and temperature control, so the main compressor can operate safely without getting into two-phase region of CO_2 during the transition. However, this control brings a huge challenge for PCHEs, because the operation conditions are dramatically changed. As shown by the black lines in Figure 17 and Figure 18, the LTR temperature encounters a temperature change up to 75℃ with a maximum temperature gradient of 0.5℃/s, which will make the PCHE suffer from the large thermal stress. The temperate gradient could be well controlled by setting a ramp load reference with a small slope or by adding a constraint on bypass valve maximum openness and opening rate. As shown by the red lines in Figure 17 and Figure 18, when a ramp load reference with 5MWe/minute (5% total load/minute) change rate is sent to the controller, the temperature gradient is reduced to 0.09℃/s, which relieves a lot the stress of PCHEs.

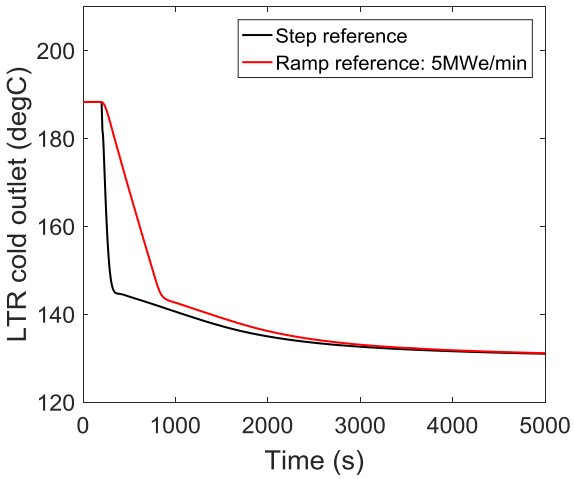

Figure 17 LTR cold flow side outlet temperature

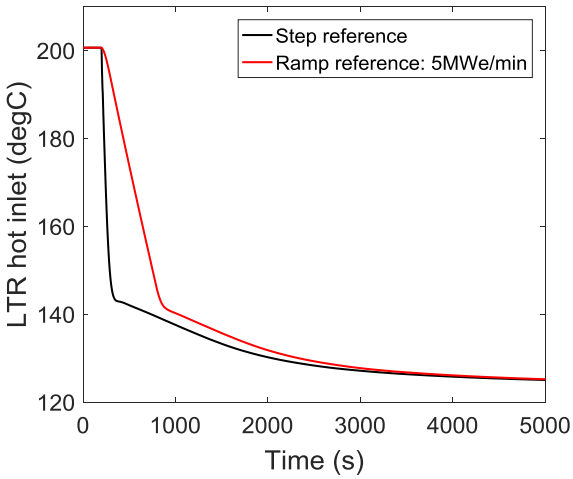

Figure 18 LTR hot flow side inlet temperature

Moreover, with a ramp load reference with 5MWe/min change rate, the load level follows closely the reference level until 53% load, then approaches the final target load level of 50%, as shown in Figure 19. This characteristics is useful for fast and frequent load regulation, where this control is able to follow the reference with a reasonable accuracy.

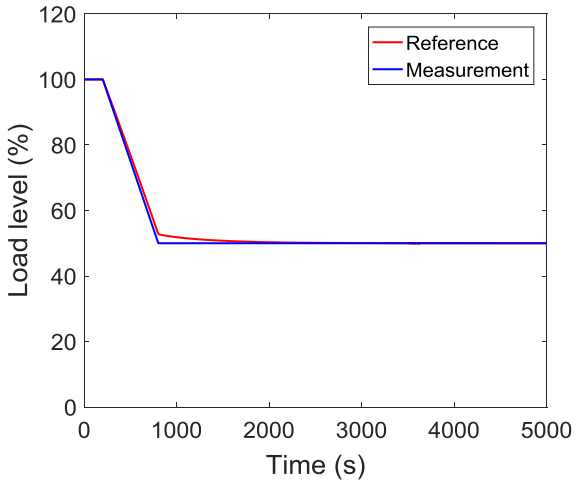

Figure 19 Reference load signal and measured power output

3. Combination of Inventory Control and HTR & Heater & Turbine Bypass Control

Based on the characteristics of inventory control and HTR & heater & turbine Bypass Control, a new control strategy is proposed by combining these two control options, which reduces the control response time and the cycle efficiency at low load level. This new proposed control strategy for part-load control works as follows:

- A load-inventory table is prepared in advance, which gives the relation between load level and the amount of inventory that needs to be discharged from the cycle, e.g. for the cycle design presented in this paper, 50% load level corresponds to a total amount of inventory discharge of 37.2 tons. This table serves as a reference for the inventory discharge when the load reference signal is given. When the inventory discharged from the cycle does not reach the reference level, the valve opens and the openness depends on the difference between reference and measurement. In the meanwhile, the openness depends also on the MCIP to avoid that the CO_2 falls below the critical point.
- HTR & heater & turbine bypass control is responsible for the part-load control during the whole

transient process.

- Inventory control takes the signal of the amount of inventory to be discharged from the load-inventory table prepared before as the control reference, and starts the same time with bypass control.

A ramp load reference from 100% load to 50% load with 5% load/minute (5MWe/minute) is given as the control reference. According to the load-inventory relation, the reference amount of inventory to be discharged is set as 37.2 tons. As shown in Figure 20, the new control strategy follows very closely the reference until 53% load then approaches 50% with a high accuracy. The high response speed comes mainly from the effective bypass control, but the inventory control also contributes to increasing the response speed. This results in the fact that the new control strategy response even faster than the bypass control alone. The efficiency curve in Figure 21 shows that the efficiency decreases monotonically until 800s, which is the period when the bypass control dominates the control process. But the efficiency level remains higher than the case with bypass control working alone, because the inventory control helps to improve the global efficiency. The minimum efficiency during the control process is 32.64%, which is much higher than 27.51% of unique bypass control.

Starting from 800s, the inventory control starts to take over the control, mainly to optimize the cycle efficiency, which brings the efficiency from 32.64% to 36.58%, which is approximately the same as the single inventory control case.

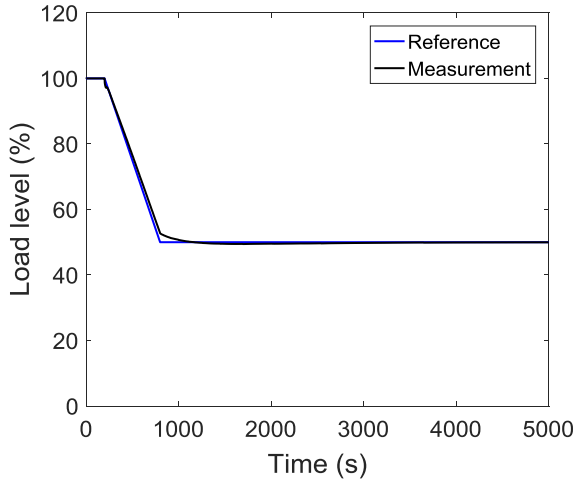

Figure 20 Reference load signal and measured power output

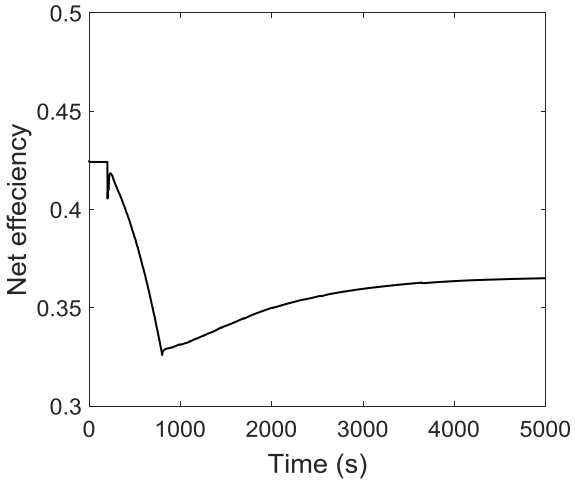

Figure 21 Cycle net efficiency

During the whole control process, the MCIP stays in the safe region. The spike in the discharge rate is a result of controller design. When the inventory discharge reference changes from 0 for 100% load to 37.2 tons for 50% load in 10 seconds, the proportional part of controller reacts immediately to the reference change, but the integral part with anti-windup design catches up with a short time delay. This results in the spike of mass flow rate. The spike can be removed by using a ramp control reference with a smaller slope.

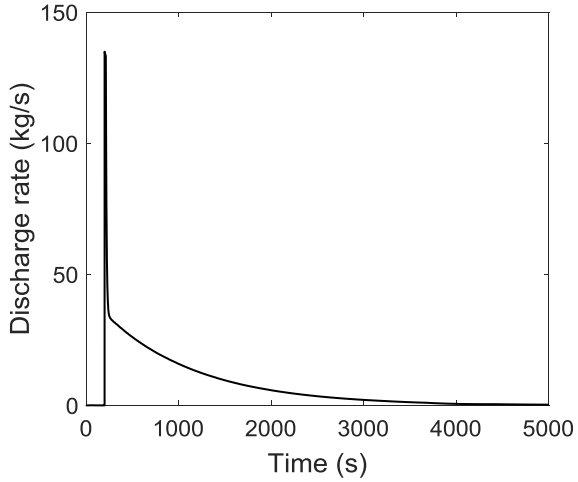

Figure 22 Discharge flow rate

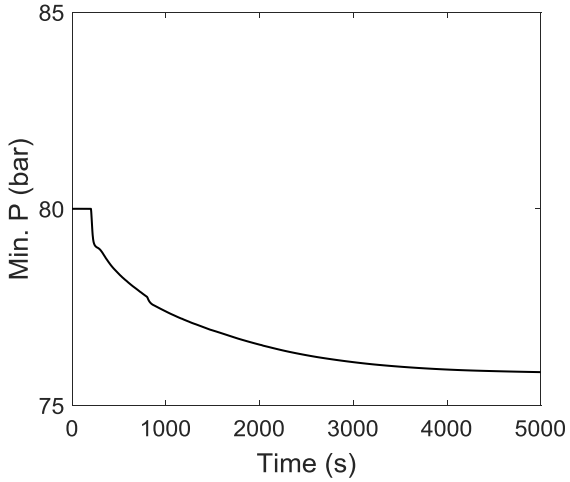

Figure 23 Main compressor inlet pressure

In Figure 24 and Figure 25, the maximum temperature change reduces to 17℃, which is much lower compared to that of single bypass control, 75℃. The temperature gradient at the beginning of control process is 0.2℃/s, which is relatively high, but it lasts only 28 seconds with a maximum temperature change of 6℃. This can be removed by further weakening the bypass impact at the beginning. Globally, the new control strategy improves the temperature performance near PCHEs, which reduces the possible stress suffered by the equipment.

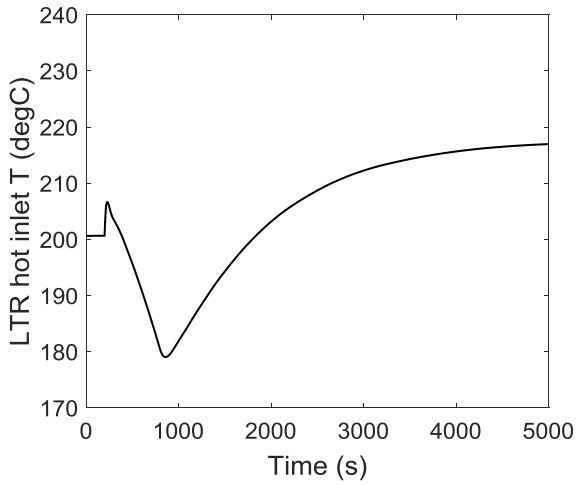

Figure 24 LTR hot flow side outlet temperature

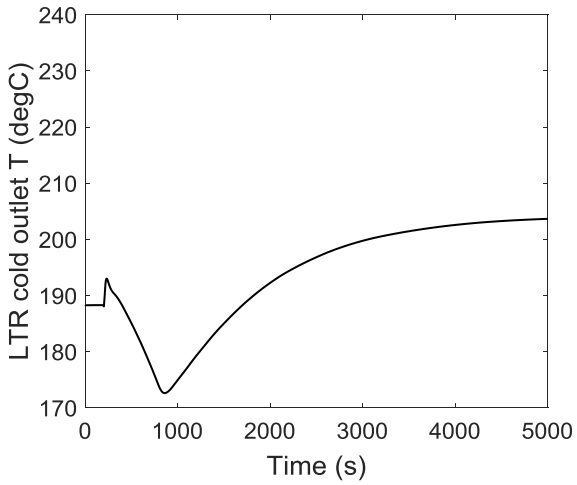

Figure 25 LTR hot flow side inlet temperature

DISCUSSION

Inventory control is able to bring the cycle load from 100% to 50% while maintain a relatively high efficiency of 37.40% with MSOT control or 38.11% with TIT control at 50% load. During inventory control, MCIP protection is necessary for the safe operation of cycle, especially for that of main compressor. In the implemented inventory control, a safe pressure zone is defined as a reference for pressure control instead of a single value, which avoids to a large extent the impact of pressure protection on the part-load control. Then flow split control and recompression compressor operation control could be used to further optimize the cycle performance.

The control conflict between MSOT control and TIT control observed during the simulation of inventory control is a challenging task, and this cannot be easily solved by control optimization. A possible solution could be realized by modifying the molten salt heat exchanger design in order to improve off-design operation. E.g. the heat exchanger design could be given based on 75% load as in Figure 26, when

operating at a load level higher than 75%, the CO_2 outlet temperature will be higher than the design value, but this can be reduced to design level by bypassing a flow from low temperature side of the cycle. As a result, two manipulated variables could be used to control two temperature, which is simpler in terms of control system design. Moreover, this design methodology also favors low load level operation, because this design could help the TIT maintain a higher temperature level than the 100% load based design, which will improve the cycle efficiency at low level.

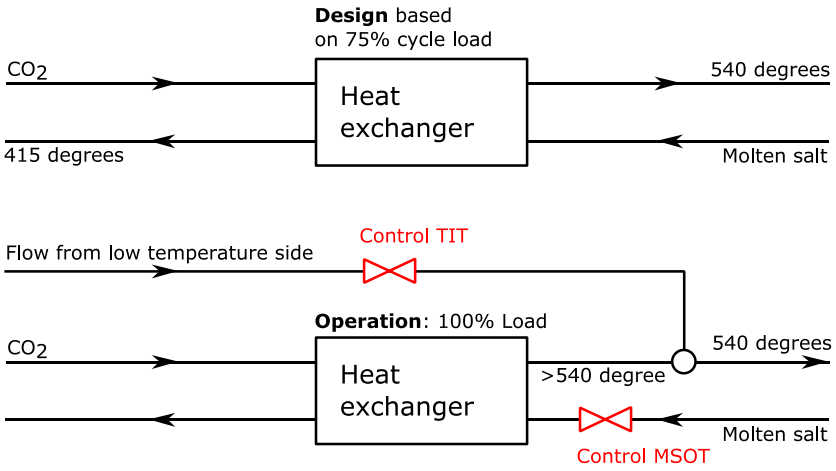

Figure 26 Optimization of molten salt off-design operation based on part-load design methodology

HTR & Heater & Turbine Bypass Control proposes a good solution for fast load variation at a large scale, with a step load reference signal from 100% to 50%, the load level could be reduced from 100% to 55% in 10s without high disturbance to the cycle, except that the PCHEs suffers from high temperature gradient. Therefore, the response time of this controller depends mainly on the maximum temperature gradient that PCHEs can sustain. When replacing the step reference with a ramp reference, due to the effective control, the load is able to follow closely the reference until 53% load, which makes it applicable for fast and frequent load regulation operation. However, the net efficiency of 27.51% at 50% load makes it not a good solution for long-term operation at lower level.

By combing inventory control and HTR & heater & turbine bypass control, the new proposed control strategy is able to achieve high response speed as bypass control and to get the same efficiency as inventory control at 50% load level. The high temperature gradient of 0.2℃/s at the beginning of control process is not good for PCHE operation, which can be solved by slowing down the bypass opening. Beyond this problem, no obvious problem is observed in the simulation, which means that this method is able to bring the load level safely from 100% to 50%.

CONCLUSION AND PERSPECTIVE

The dynamic model of recompression supercritical CO_2 Brayton cycle built in Dymola® is a full closed loop model with detailed equipment on-design and off-design modeling. The sub-models integrated in the cycle model are based on the fundamental physical laws and well-developed models found in the open literature. Therefore, this model is believed to be able to reflect realistic cycle transient phenomena.

Dymola® is a good platform for dynamic modeling and simulation, but it is found that it is difficult for the solver integrated in Dymola® to solve highly non-linear equation systems with a large amount of equations (e.g. the cycle model presented in this work has nearly 13000 equations), especially for supercritical CO_2 systems where the CO_2 thermodynamic properties are highly non-linear near the critical point. It is found that during cycle showdown, when the whole cycle operation conditions approach critical point, the solver is difficult to reach convergence.

Based on this dynamic model, part-load scenario from 100% load to 50% load is studied. Two control options are simulated and analyzed. Inventory control could maintain a relatively high efficiency during load reduction, but its response to step reference is very slow, and it is risky to accelerate its response because a high discharge rate can easily bring the minimum pressure below critical pressure, which is

inacceptable for the operation of main compressor. Moreover, during inventory control, a 50% load reduction leads to a 24% inventory discharge, which requires a huge buffer tank and a bigger one for lower load requirement. This characteristic of inventory control makes it not suitable for small load level, e.g. smaller than 50%. This brings a big challenge for S-CO_2 Brayton cycle minimum operation. HTR & Heater & Turbine Bypass Control reacts much faster than inventory control and it has acceptable influence on cycle operation conditions if the bypass rate could be well controlled. But this control has a much smaller net efficiency at low load level. Moreover, it brings a huge challenge for the PCHEs' off-design operation. The impact of large temperature change rate on PCHEs should be carefully evaluated to avoid any damage on the equipment. Based on the characteristics of these two control options, a new control strategy is proposed by combining these two control options, which inherits the control response speed of bypass control and in the meanwhile the high net cycle efficiency of inventory control at low load level. The improved cycle part-load control performance brought by the combined control strategy shows the potential and necessity to conduct detailed transient study for other part-load control options, such as turbine bypass control, turbine inlet valve control and load control by recirculating heater outlet flow back into heater, in order to understand their strengths and problems. Once these studies are done and these different control options are understood, an overall optimal control strategy will be proposed which could operate on all the range of load level.

Finally, for molten salt heated supercritical CO_2 cycle, in order to deal with the control conflict between TIT and MSOT in parallel, the part-load design methodology will be used in the next work to optimize the heat exchanger design for off-design operation. Based on this design, a new manipulated variable is introduced which simples the controller design for TIT and MSOT control. This will solve the conflict between molten salt storage management and cycle performance, then to improve the global cycle management.

REFERENCES

Afzal N. Friction Factor Directly From Transitional Roughness in a Turbulent Pipe Flow. Journal of Fluids Engineering, 2007, 129(10):1255-1267.

Ahn Y, Bae S J, Kim M, et al. Review of supercritical CO 2, power cycle technology and current status of research and development. Nuclear Engineering & Technology, 2015, 47(6):647-661.

Aungier R H, Farokhi S. Axial-Flow Compressors: A Strategy for Aerodynamic Design and Analysis. ASME Press, 2003.

Brown G O. The History of the Darcy-Weisbach Equation for Pipe Flow Resistance. American Society of Civil Engineers, 2002, 38(2003):34-43.

Carstens N A. Control strategies for supercritical carbon dioxide power conversion systems. Massachusetts Institute of Technology, 2007.

Chen, N.H., 1979, An Explicit Equation for Friction Factor in Pipe, Ind. Eng. Chem. Fund., Vol. 18, pp. 297-297.

Dyreby J J. Modeling the Supercritical Carbon Dioxide Brayton Cycle with Recompression. Doctor of Philosophy, University of Wisconsin-Madison, 2014.

Dostal, Vaclav. A supercritical carbon dioxide cycle for next generation nuclear reactors. Massachusetts Institute of Technology, 2004, 154(3):265-282.

Gupta S, Saltanov E, Mokry S J, et al. Developing empirical heat-transfer correlations for supercritical CO 2, flowing in vertical bare tubes. Nuclear Engineering & Design, 2013, 261(8):116-131.

Hesselgreaves J E. Compact Heat Exchangers. McGraw-Hill Book Company, Inc, 2001.

Idel'chik, I. E, Steinberg, M. O, Malyavskaya, Greta R, et al. Handbook of hydraulic resistance. Hemisphere, 1966.

Nikuradse J. Laws of flow in rough pipes. Technical Report Archive & Image Library, 1933.

Shockling M A, Allen J J, Smits A J. Roughness effects in turbulent pipe flow. Journal of Fluid Mechanics, 2006, 564(564):267-285.

Sletfjerding E. Friction Factor in Smooth and Rough Gas Pipelines. Dr.Ing. thesis, Norwegian University

of Science and Technology, Trondheim, 1999.

Tournier J M, El-Genk M S. Axial flow, multi-stage turbine and compressor models. Energy Conversion & Management, 2010, 51(1):16-29.